Rethinking Pseudocapacitance: A Way to Harness Charge Storage of Crystalline RuO2

Ankita Jadon, Sagar Prabhudev, Gaëtan Buvat, Sai Gourang Patnaik, Mehdi Djafari-Rouhani, Alain Estève, Daniel Guay, David Pech

Rethinking Pseudocapacitance: a Way to Harness Charge Storage of Crystalline RuO_2

Ankita Jadon,[§,†] Sagar Prabhudev,[‡,†] Gaëtan Buvat,[‡] Sai Gourang Patnaik,[§]

Mehdi Djafari-Rouhani,[§] Alain Estève,[§,] Daniel Guay,[‡,*] David Pech[§,*]*

§ LAAS-CNRS, Université de Toulouse, CNRS, 31400 Toulouse, France.

‡ INRS-Énergie, Matériaux et Télécommunications, 1650 Boulevard Lionel Boulet, Varennes, Québec H3A 3C2, Canada.

† = these authors contributed equally to this work

* Alain Estève: aesteve@laas.fr, Daniel Guay: guay@emt.inrs.ca, David Pech: dpech@laas.fr

ABSTRACT. With its huge pseudocapacitance and excellent stability, ruthenium dioxide (RuO_2) is considered to be one of the best electrode materials for supercapacitors. However, such properties are only obtained with hydrous RuO_2 in an amorphous phase, limiting the range of possible deposition techniques. Herein we report a detailed understanding of reactions of protons (H^+) occurring in crystalline RuO_2 with regard to its orientation using density functional theory. In particular, we show that migration pathways are energetically favorable along the [001] direction, leading to a deeper H^+ penetration within the bulk of the active material and a much higher charge storage ability.

TOC GRAPHICS.

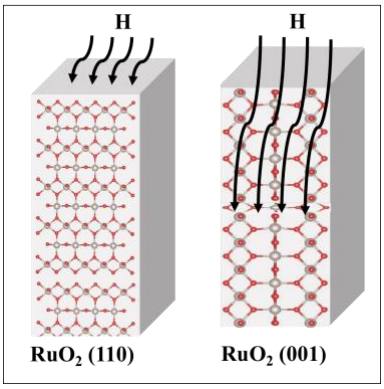

KEYWORDS. Hydrogen diffusion; Supercapacitor; Ruthenium dioxide; Cathodic polarization; Charge Storage; DFT.

In the past ten years, electrochemical capacitors, also called supercapacitors, have gained exceptional significance as electrochemical energy storage devices for applications requiring short load cycle and high reliability. Unlike batteries, supercapacitors exhibit high power capability[1] and excellent chemical stability upon cycling.[2-5] However, they store less energy than batteries because of their charge storage mechanism based on interfacial reactions between the electrode and the electrolyte. Pseudocapacitive materials offer both high power and high energy density and blur the distinction between conventional double-layer supercapacitors and batteries. These electrode materials display the electrochemical signature of a capacitive electrode (i.e. a linear dependence of the charge stored with changing potential within the window of interest) but their charge storage originates from faradaic electron-transfer mechanisms.[6] Because these redox reactions are not accompanied by a crystallographic phase transition, pseudocapacitive materials can also exhibit very long lifetime. With its ideal pseudocapacitive behaviour and metallic conductivity, hydrous forms of ruthenium dioxide ($RuO_2.xH_2O$) by far dominate all other pseudocapacitive materials with the highest specific capacitance. Even if its high cost has limited its development for large-size supercapacitors, this material is very promising for micro-supercapacitors at the dawn of the Internet of Things (IoT).[7] Its redox pseudocapacitance is ascribed to a series of fast and reversible electron transfer reactions coupled with adsorption and absorption of protons on the surface and in the bulk, respectively, involving several oxidation states of Ru, which can be expressed as follows:

$$RuO_x(OH)_y + \delta H^+ + \delta e^- \leftrightarrow RuO_{x-\delta}(OH)_{y+\delta}$$

with $0 < x < 2$. Despite its remarkable properties, hydrous forms of ruthenium dioxide $RuO_2.xH_2O$ tested in diluted sulfuric acid solutions has a restricted voltage range of ca. 1V because of inevitable water decomposition at higher potentials. Moreover, hydrous form of ruthenium dioxide

is mainly obtained by electrodeposition, which excludes a large number of other deposition techniques like PVD (Physical Vapor Deposition). The origin of the anomalous high pseudocapacitance of hydrated ruthenium dioxide compared with anhydrous RuO_2 is still obscure. Anhydrous form of RuO_2 has high crystallinity while its completely hydrous form, $RuO_2.xH_2O$, is amorphous with no characteristic XRD (X-Ray Diffraction) patterns. Most theoretical and experimental investigations on anhydrous ruthenium dioxide were performed on the stable (110) surface of the rutile-like RuO_2 with poor electrochemical performances for energy storage applications.[8-13]

In this work, we investigate the bulk adsorption, migration and penetration of hydrogen in a new anisotropic RuO_2 (001) orientation from DFT-based calculations, and compare the results with conventional RuO_2 (110). The results are discussed in the light of experimental electrochemical measurements performed on RuO_2 (001) and (110) under cathodic polarization. For the first time, we show that higher pseudocapacitance can be obtained in anhydrous RuO_2 with a suitable crystalline orientation through an enhanced hydrogen insertion and accumulation in the electrode material.

Figure 1 presents an overall picture of DFT calculations performed on the penetration of hydrogen into RuO_2 (110) and (001) surfaces including structural as well as energetic aspects. On both surfaces, we have established all adsorption sites for hydrogen (see Supporting Information). On the conventional RuO_2 (110) surface, our DFT calculations show that hydrogen adsorbs with an energy of -0.95 eV. This adsorption is accompanied with a strong charge transfer towards the oxygen atom giving to the hydrogen a proton-like behaviour, hydrogen charge +0.61 e-. A similar behaviour is found for the (001) surface, but with a lower adsorption energy, -0.55 eV, the hydrogen charge being +0.64 e-.

From both surface adsorption sites, the first step for penetration in the immediate subsurface layer is now addressed. For the (110) surface, the diffusion barrier to accomplish such a migration is +1.7 eV (see Figure 1), which is equivalent to values previously reported in the literature in bulk calculations, following the same crystallographic direction.[10] Adsorption energy in the sub-layer is still high, but with a slightly lower adsorption energy -0.82 eV. Both these values make the process unlikely from kinetic and thermodynamic stand points, particularly for what concerns the activation barrier that will hinder migration of hydrogen at room temperature. This may explain the poor pseudocapacitance achieved experimentally. Note that proton like behaviour of the migrating hydrogen is conserved, with a net charge of +0.61 e-. In contrast, for the (001) surface, the activation barrier for penetration is largely lower, 0.43 eV (Figure 1), which corresponds to a well-activated process at room temperature for typical vibration frequencies. As in the (110) subsurface, hydrogen conserves its proton like behaviour (+0.64 e-), and the pathway is slightly endothermic with a loss of 0.31 eV energy (*i.e.*, adsorption energy is now -0.24 eV). Towards inner layers, for both surfaces, the tendency is to converge rapidly to bulk regime, in terms of adsorption energy (-0.11 eV), with progressively lower bond strength. From the surface, in the (001) case, two migration steps are needed before obtaining bulk regime (-0.55; -0.24; -0.12 eV adsorptions, respectively). For the (110) surface, three migrations are necessary in order to converge to bulk kind of adsorption (-0.95; -0.82; -0.29; -0.11 eV adsorptions, respectively). Starting from the sub-layer, all configurations of adsorption are similar in all cases (irrespective of the surface), as expected from local topology and symmetries: hydrogen is always bonded to one oxygen atom (1.00 Å bond length) sharing a hydrogen bond with a second nearest oxygen atom (at 1.82 Å). A Bader charge analysis indicates that the hydrogen charge is always in the +0.6 e- range. We would like to point out that the surface effects are appreciable down to the fourth (10.4 Å) and the third

(5.3 Å) layers for (110) and (001) surfaces, respectively. Note that activation barriers and charge transfers values are not affected by surface and subsurface presence and correspond to bulk values. Given the very low activation barrier for migration in the case of the (001) surface (surface to the first layer: 0.43 eV), we can assume that, along the [001] channel orientation, hydrogen migration is relatively faster and reaches the bulk migration regime quickly (post 5.23 Å depth). In this bulk regime, from calculated activation barriers and prefactors, we obtain a diffusion coefficient at 300 K of 4.0×10^{-30} and 1.1×10^{-6} cm^2/s along [110] and [001], respectively (see Supporting Information for calculation details). Altogether, the dramatic difference in diffusion coefficients indicate that controlling crystalline orientation during deposition should have a large impact on the storage density of purely crystalline RuO_2 electrodes.

In order to experimentally corroborate these theoretical findings, the ease of migration of hydrogen atoms into RuO_2 (001) and RuO_2 (110) structures has been electrochemically investigated in a potential region where only chemisorption of atomic hydrogen ($H^+ + e^- \rightarrow H_{ads}$) is taking place.[14,15] For this purpose, it was indispensable to obtain monocrystalline thin films of RuO_2. Two types of RuO_2 electrodes along (001) and (110) were therefore epitaxially grown onto a TiO_2 (001) and MgO single-crystal substrates using a pulsed laser deposition (PLD) of a metallic Ru target in the presence of oxygen (100 mTorr O_2, see Supporting Information for details).

Figure 2a illustrates the X-ray diffraction (XRD) pattern of as-deposited RuO_2 (001) thin film, with an estimated thickness of 34 nm. The noticeable peak at 63° is the (002) diffraction peak corresponding to (001)-oriented TiO_2 substrate. The $K\beta$ reflection of (002) TiO_2 is also seen at 56°. The discernible peak at 59.5º is the (002) reflection corresponding to rutile RuO_2, substantiated also by the fact that the observed lattice-parameters (c = 3.1 Å) remain closely similar to the reported values (c = 3.107 Å; JCPDS card no. 40-1290). As expected, within the scanned range

shown in Figure 2a, prominent other RuO_2 peaks at 54° (211), 59° (220) and 66° (112) are absent. This is indicative of the single-crystal nature of the RuO_2 thin-film, successfully grown along the [001] oriented perpendicularly to the substrate surface. The surface roughness (RMS), estimated from atomic force microscopy (AFM) images, is about 4.9 nm, and appears to be well-maintained even after polarization (4.5 nm, Figure 2b and SI Figure S3).

Both RuO_2 electrodes were polarized at +0.1 V vs. RHE for different durations to allow H-chemisorption without being in the hydrogen evolution reaction (HER) region, and investigate proton intercalation within the oxide structure. Between each polarization, a set of cyclic voltammograms (CVs), carried out using same experimental conditions, were performed between +0.1 and +1.25 V vs. RHE at 100 mV/s. The polarization did not seem to affect the electrochemical behaviour of the RuO_2 (110), even after a long-term polarization. However, as expected from DFT calculations, a difference in the CVs shape was observed for RuO_2 (001) sample before and after polarization at +0.1 V vs. RHE (Figure 3). The voltammetric charge increases with increasing hold time of polarization in the potential window where H-chemisorption occurs. Interestingly, this effect was not observed when the electrode was polarized at +0.7 V vs. RHE (see SI Figure S6), i.e. in the potential windows where redox pseudocapacitive reactions take place and no chemisorption (and therefore no intercalation) of hydrogen occurs. This further confirms the origin of charge storage at low potential in RuO_2 (001).

Figure 4a shows the difference of voltammetric charge between non-polarized and polarized RuO_2 as a function of the holding time at +0.1 V vs. RHE. The charge related to insertion of protons increases rapidly to reach a plateau at around 0.09 mC after 20 s hold-duration. Figure 4b shows the evolution of current vs. time during polarization at +0.1 V vs. RHE for RuO_2 (001). Noticeably, all profiles coincide onto one another whatever the duration of polarization. This is

indicative that H-chemisorption proceeds with the same kinetics and is not affected by history of the electrode. From the integration of the curve (see inset Figure 4b), a reductive charge of around 0.09 mC has been estimated, i.e. identical to the oxidative charge obtained from CVs (Figure 4a). Therefore, the H-chemisorption and diffusion process in the material seems to be reversible: the charge associated with H diffusion in the material is totally restored upon reversal of potential. Hence, these electrochemical experiments provide experimental evidence of the lower activation barrier for diffusion of protons in RuO_2 (001) compared with RuO_2 (110), resulting in much higher charge storage ability.

In conclusion, we have shown from DFT-based calculations that higher pseudocapacitance can be obtained in anhydrous RuO_2 with a suitable crystalline orientation through an enhanced hydrogen insertion and accumulation mechanism in RuO_2 (001) compared with RuO_2 (110). The penetration of hydrogen proceeds via H^+ reduction, adsorption of atomic hydrogen accompanied by a strong charge transfer towards the oxygen atom (+0.64 e^-) and proton migration from RuO_2 surfaces to the depth of RuO_2 (001). We then successfully synthesized by PLD single-crystalline RuO_2 (001) and RuO_2 (110) thin films, and used them as model materials for experimental validation. Both single crystal thin films were polarized at +0.1 V vs. RHE for different durations and, as expected, the voltammetric charge increases with increasing hold time of polarization for the RuO_2 (001). These electrochemical results perfectly match the predicted DFT calculations and bring new insights towards the charge storage mechanism occurring in pseudocapacitive materials. It paves the way to engineer pseudocapacitive electrode thin films with enhanced electrochemical properties, providing opportunities to enhance the performance of micro-supercapacitor electrodes.

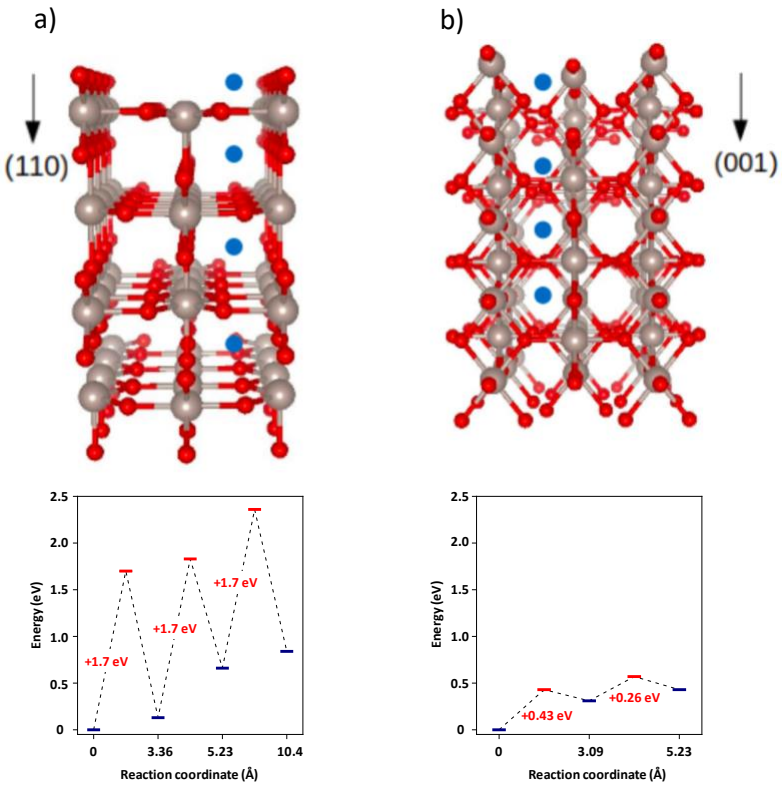

Figure 1. a) Images showing proton migration from RuO_2 surfaces to the depth of RuO_2 (110) and b) RuO_2 (001). It can be seen that the cage for RuO_2 (001) is relatively smaller compared to RuO_2 (110). Grey: Ru; Red: O; Blue: H.

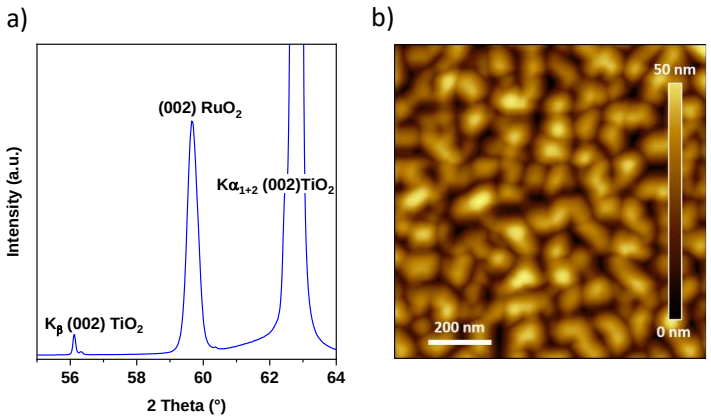

Figure 2. Structural characterization of as-desposited RuO_2(001)/TiO_2(001) film: (a) XRD pattern featuring diffraction peaks related to RuO_2 (hkl), JCPS card #40-1290. (b) AFM image illustrating surface topography of RuO_2 film.

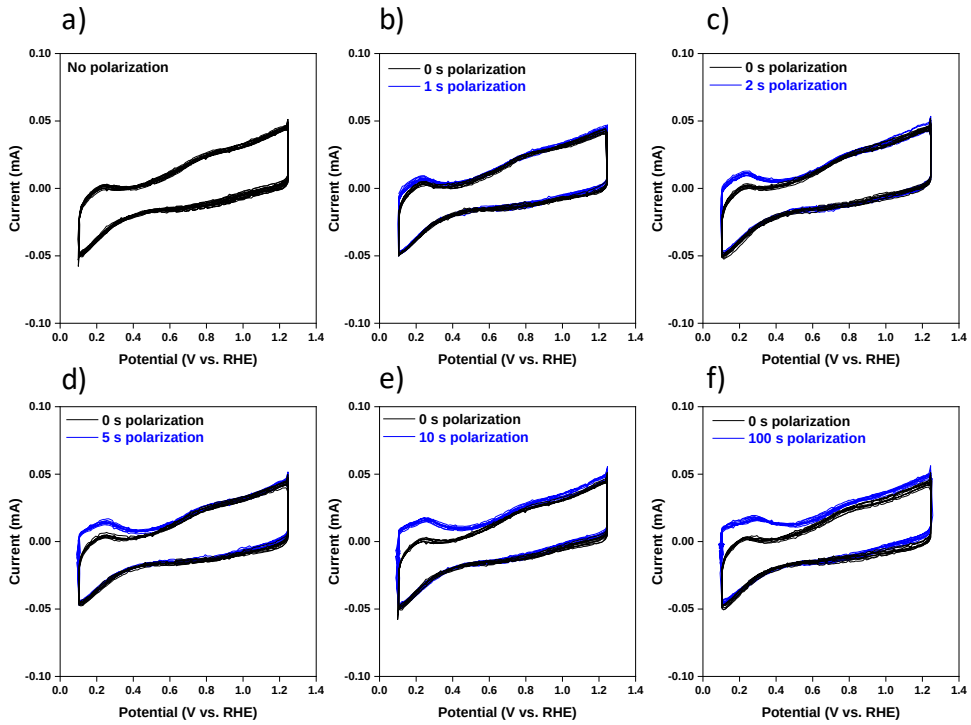

Figure 3. Cyclic voltammogram (CV) profiles of RuO_2 (001) before (black) and after (blue) polarization at +0.1 V vs. RHE for a) 0 s, b) 1 s, c) 2 s, d) 5 s, e) 10 s and f) 100 s. All CVs were performed 10 times at 100 mV/s in deaerated 0.5 M H_2SO_4.

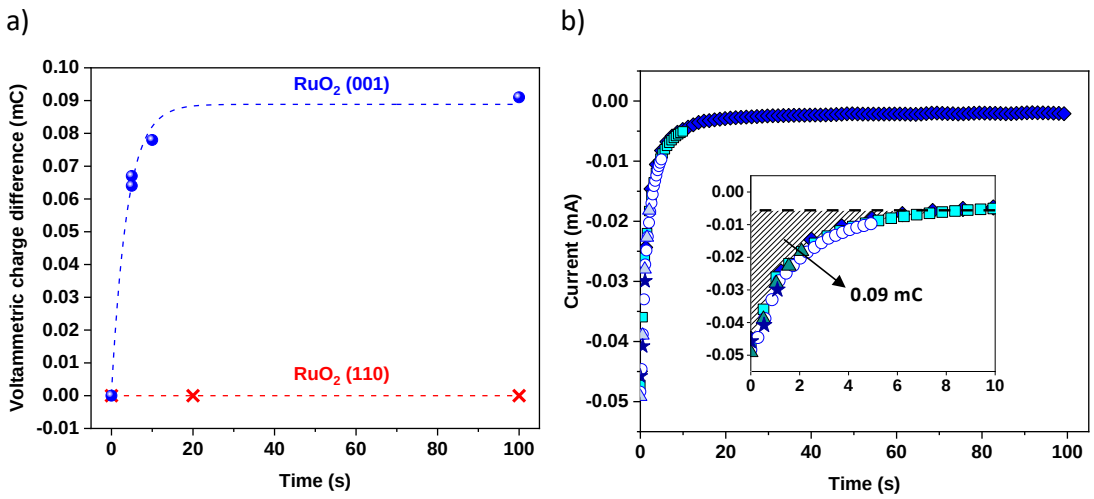

Figure 4. (a) Voltammetric charge difference between non-polarized and polarized RuO_2 (110) and (001) as a function of polarization duration (i.e. hold-time at +0.1 V vs. RHE). (b) Potentiostatic polarization curves of RuO_2 (001) for different polarization durations (1, 2, 5, 10 and 100 s). Inset shows the magnified region from 0 to 10 s with a similar charge of 0.09 mC (shaded area).

ASSOCIATED CONTENT

Supporting Information.

Experimental methods (electrode fabrication, structural characterizations, electrochemical characterizations), computational details, adsorption sites and diffusion coefficients. This material is available free of charge via the Internet at http://pubs.acs.org.

AUTHOR INFORMATION

Corresponding Authors

* Alain Estève: aesteve@laas.fr, Daniel Guay: guay@emt.inrs.ca, David Pech: dpech@laas.fr

Notes

The authors declare no competing financial interests.

The data that support the plots within this paper can be obtained free of charge from Zenodo via https://zenodo.org.

ACKNOWLEDGMENT

This work was granted access to the high-performance computing resources of CALMIP supercomputing center. D. Pech acknowledges the support from the European Research Council (ERC, Consolidator Grant, ERC-2017-CoG, Project 771793 3D-CAP). D. Guay acknowledges the support of the Natural Science and Engineering Research Council (NSERC) of Canada and the Canada Research Chair (CRC) program.

REFERENCES

(1) Pech, D.; Brunet, M.; Durou, H.; Huang, P.; Mochalin, V.; Gogotsi, Y.; Taberna, P. L.; Simon, P. Ultrahigh-Power Micrometre-Sized Supercapacitors Based on Onion-Like Carbon. *Nat. Nanotechnol.* **2010**, *5*, 651-654.

(2) Wang, F.; Wu, X.; Yuan, X.; Liu, Z.; Zhang, Y.; Fu, L.; Zhu, Y.; Zhou, Q.; Wu, Y.; Huang, W. Latest Advances in Supercapacitors: From New Electrode Materials to Novel Device Designs. *Chem. Soc. Rev.* **2017**, *46*, 6816-6854.

(3) Liang, Z.; Zhao, R.; Qiu, T.; Zou, R.; Xu, Q. Metal-Organic Framework-Derived Materials for Electrochemical Energy Applications. *EnergyChem* **2019**, *1*, 100001.

(4) Zhang, G.; Xiao, X.; Li, B.; Gu, P.; Xue, H.; Pang, H. Transition Metal Oxides with One-Dimensional/One-Dimensional-Analogue Nanostructures for Advanced Supercapacitors. *J. Mater. Chem. A* **2019**, *5*, 8155-8186.

(5) Ge, J.; Wang, B.; Zhang, Q.; Lu, B. Nature of $FeSe_2$/N-C Anode for High Performance Potassium Ion Hybrid Capacitor. *Adv. Energy Mater.* **2020**, *10*, 1903277.

(6) Brousse, T.; Bélanger, D.; Long, J. W. To Be or Not To Be Pseudocapacitive? *J. Electrochem. Soc.* **2015**, *162*, A5185-A5189.

(7) Kyerematen, N. A.; Brousse, T.; Pech, D. Microsupercapapacitors as Miniaturized Energy-Storage Components for On-Chip Electronics. *Nat. Nanotechnol.* **2017**, *12*, 7-15.

(8) Sun, Q.; Reuter, K.; Scheffler ; M. Hydrogen Adsorption on RuO_2(110): Density-Functional Calculations. *Phys. Rev. B* **2004,** *70*, 235402.

(9) Knapp, M.; Crihan, D.; Seitsonen, A. P.; Lundgren, E.; Resta, A.; Andersen, N.; Over, H. Complex Interaction of Hydrogen with the RuO_2(110) Surface. *Phys. Rev. C* **2007,** *111*, 5363-5373.

(10) Kim, S.; Lai, W. Hydrogen Diffusion Behavior and Vacancy Interaction Behavior in OsO_2 and RuO_2 by Ab Initio Calculations. *Comput. Mater. Sci.* **2015,** *102*, 14-20.

(11) Zakaryan, H. A.; Kvashnin A. G.; Oganov, A. R. Stable Reconstruction of the (110) Surface and Its Role in Pseudocapacitance of Rutile-Like RuO_2. *Sci. Rep.* **2017**, *7*, 10357.

(12) Rao, R. R.; Kolb, M. J.; Halck, N. B.; Pedersen, A. F.; Mehta, A.; You, H.; Stoerzinger, K. A.; Feng, Z.; Hansen, H. A.; Zhou, H.; Giordano, L.; Rossmeisl, J.; Vegge, T.; Chorkendorff, I.; Stephens, I. E. L.; Shao-Horn, Y. Towards Identifying the Active Sites on RuO_2(110) in Catalyzing Oxygen Evolution. *Energy Environ. Sci.* **2017**, *10*, 2626-2637.

(13) Dahal, A.; Mu, R.; Lyubinetsky, I.; Dohnálek, Z. Hydrogen Adsorption and Reaction on RuO_2(110). *Surf. Sci.* **2018**, *677*, 264-270.

(14) Blouin, M.; Guay, D. Activation of Ruthenium Oxide, Iridium Oxide, and Mixed Ru_xIr_{1-x} Oxide Electrodes during Cathodic Polarization and Hydrogen Evolution. *J. Electrochem. Soc.* **1997,** *144*, 573-581.

(15) Chabanier, C.; Guay, D. Activation and Hydrogen Absorption in Thermally Prepared RuO_2 and IrO_2. *J. Electroanal. Chem.* **2004,** *570*, 13-27.